Vapor−Solid Growth of Sn Nanowires: Growth Mechanism and Superconductivity

Yung-Jung Hsu and Shih-Yuan Lu*

Department of Chemical Engineering, National Tsing-Hua University, Hsin-Chu, Taiwan 30043, Republic of China

Received: August 12, 2004; In Final Form: January 11, 2005

A noncatalytic and template-free vapor transport process has been employed to prepare single-crystalline Sn nanowires with diameters of 10−20 nm. The growth of one-dimensional Sn nanowires follows the mechanism similar to the vapor−solid (V−S) mechanism. Two-dimensional square-shaped nanostructures were also found to form in the region of lower deposition temperatures. The rich morphology may be attributed to the competition in growth rate among different crystallographic planes. Structural characterization with high-resolution transmission electron microscopy showed that the nanowires and nanosquares grew in a preferential direction of [200]. The superconducting transition temperatures for Sn nanowires and Sn nanosquares were about 3.7 K, which was very close to that of bulk β-Sn. Magnetization measurements showed that the critical magnetic fields for both Sn nanowires and Sn nanosquares increased significantly as compared to that of bulk Sn.

Introduction

One-dimensional nanostructures have drawn much research attention in recent years due to their novel properties and potential applications in a number of different fields.[1,2] Among others, metal nanowires can be used as the functional components and interconnects in electronic devices, magnetic devices, and nanosensors.[3−7] For preparation of metal nanowires, the template-assisted procedure is commonly used for its good dimension control.[8−12] The templates, such as polycarbonate and anodic alumina membranes, possess porous channels of controllable size, utilization of which in nanowire fabrication offers the advantages of predefined 1-D morphology and controllable wire diameter. However, there still exist some intrinsic shortcomings and limitation with the template-directed method. First, metal nanowires synthesized with the assistance of porous templates usually possess polycrystallinity, although it is possible to generate single-crystalline metal nanowires by carefully controlling the reaction conditions.[8,9] Second, removal of the native templates to get free-standing nanowires for further use is troublesome and time-consuming, not to mention the possible contamination of the excess solvents involved in dissolving the templates. Last, the imperfection in wire morphology, such as the surface roughness and nonuniformity in diameter, inheriting from the imperfection of the template channels is also a concern. Normally, it is difficult to produce porous templates with straight and smooth channels.

We reported here the fabrication of single-crystalline tin (Sn) nanowires with a noncatalytic and template-free physical vapor deposition (PVD) process and the relevant structural and superconducting characterizations. Vapor-phase synthesis of one-dimensional nanostructures of metals without the help of templates and catalysts has not been studied extensively. Direct syntheses of high-quality tungsten nanowires and zinc nanobelts in gas-phase system were reported recently.[13,14] Besides, there were a few articles discussing vapor-phase based synthesis and characterization of metal whiskers in the 1960s, and no conclusive results were obtained for relevant growth mechanisms and structural characterizations to boost further development toward metal nanowires.[15] Our synthesis was based on thermal evaporation of bulk Sn balls under controlled conditions, without the presence of templates and catalysts. Bulk Sn balls were placed at the center of a quartz tube, heated in a horizontal tube furnace. The temperature, pressure, and evaporation time of the operation were controlled. During the process, the products were deposited onto the Si(100) substrates placed at the downstream end of the quartz tube. The as-deposited products were characterized and analyzed with X-ray diffraction (XRD), scanning electron microscopy (SEM), high-resolution transmission electron microscopy (HRTEM), X-ray photoelectron spectroscopy (XPS), and superconducting quantum interference device (SQUID) magnetometer.

Experimental Section

PVD Process for Preparation of Sn Nanowires. One-dimensional nanowires and two-dimensional nanosquares of Sn were grown in a hot-wall quartz tube reactor with the system pressure maintained at 30 Torr and the nitrogen carrier gas flow rate set at 200 sccm. The source material, pure Sn balls were first cleaned in HCl solution for 20 min to remove the surface oxide layer, followed by heating to 700 °C to generate Sn vapors in the reactor. Silicon substrates, Si(100), were cleaned in an ultrasonic bath of acetone for 20 min, HF solution for 1 min, and deionized water for 10 min. The Sn vapors condensed to crystallize on the Si(100) substrates to form Sn nanowires and nanosquares at deposition temperatures of 210 and 180 °C, respectively. It should be noted that with carefully controlling the reactor condition at the end of the evaporation process, we successfully obtained metallic Sn nanowires free of oxidation. As the evaporation process ceased, the system was allowed to cool to room temperature with nitrogen kept flowing to protect the products from oxygen attack. Afterward, the products were taken out of the reactor for preservation and further characterizations. This way, we successfully avoided the possible oxidation of Sn nanowires at high temperatures. In fact, if the

* Corresponding author: SYLu@mx.nthu.edu.tw

10.1021/jp046354k CCC: $30.25
Published on Web 02/12/2005

system was allowed to cool in air with the products exposed to ambient air at high temperatures, a minor amount of SnO_x was also detected. The oxidation process of Sn in ambient air was found to be highly kinetically controlled, accomplished by diffusion of oxygen.[16] The diffusion coefficient of oxygen in SnO_2 at 298 K was estimated to be about 10^{-33} cm^2 s^{-1}, a relatively small value, indicating that the oxidation of Sn in air at room temperature is a very slow process.[17] Thin films, nanoparticles, and nanowires of Sn had also been reported to be stable in ambient air, and no oxides formed unless the products were thermally treated in air at temperatures above 200 °C.[16−18] In this work, the as-prepared Sn nanowires were protected from possible oxygen attack at high temperatures by the inert nitrogen flow, and the Sn nanowires collected at room-temperature remained stable due to the very slow oxidation rate at room temperature in ambient air.[17]

Characterization. The morphology and dimension of the as-deposited products were examined with scanning electron microscope (SEM, Hitachi, S-4700). The compositional information was obtained with X-ray photoelectron spectroscopy (XPS, Physical Electronics, ESCA PHI 1600). A charge correction based on the standard reference of the C 1s (284.5 eV) signal was applied to all XPS peaks in Sn 3d and Sn 3p. The crystallographic structures of the resulting deposits were analyzed using X-ray diffraction (XRD, Mac Sience, MXP18) and high-resolution transmission electron microscope (HRTEM, JEOL, JEM-4000EX). Magnetization measurements of the samples were carried out at low temperatures using a superconducting quantum interference device magnetometer (SQUID, Quantum Design, MPMS5).

Results and Discussion

Thermal evaporation of bulk Sn balls (melting point: 232 °C) at 700 °C in nitrogen environment for 4 h resulted in white and fluffy products formed on the surface of the Si(100) substrates. SEM observations revealed that the products consisted of a large quantity of nanowires with typical diameter of 10−20 nm and length up to several micrometers, as shown in Figure 1a. XRD pattern in Figure 1b confirmed the crystal structure of tetragonal β-Sn with lattice constants of $a = 5.804$ Å and $c = 3.169$ Å. Here, a small lattice shrinkage, characteristic of nanosized crystals, as compared with the corresponding values of reference bulk β-Sn of $a = 5.831$ Å and $c = 3.182$ Å (JCPDS powder diffraction file number of 04−0673), was observed. Note also that there were no peaks attributable to tin oxide, indicating the success of our process in avoiding the commonly encountered oxidation problem for most metal materials preparation processes.

The Sn 3d XPS spectrum for the as-deposited Sn nanowires was shown in Figure 2. The Sn 3d XPS spectrum exhibited signals consistent with the presence of metallic Sn state with the binding energies of 485.0 and 493.5 eV for the $3d_{5/2}$ and $3d_{3/2}$ peaks, respectively,[19] confirming again the existence of metallic Sn and absence of tin oxide in the samples.

A typical TEM image of the free-standing Sn nanowires was shown in Figure 3a. The nanowires imaged here were with a rather uniform diameter of about 20 nm and no heads were observed at the tips of the nanowires. The dot pattern of the inserted selected area electron diffraction (SAED) image showed that the Sn nanowires grew as a single crystal. The SAED pattern can be indexed to a tetragonal phase of Sn recorded along the [001] zone axis, which is consistent with the XRD pattern. The diameter of the nanowire was quite uniform along the length of nanowire, which can be observed in a typical low-magnification TEM image shown in Figure 3b.

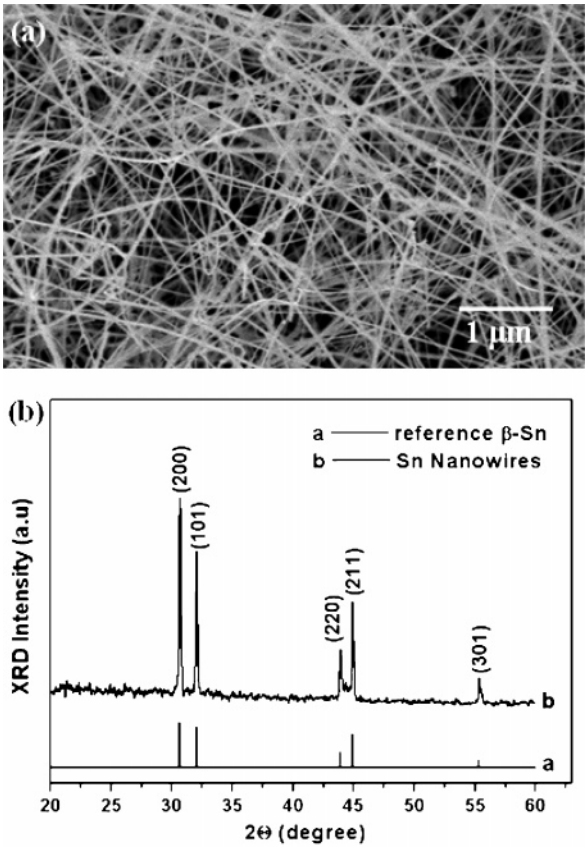

Figure 1. (a) Top view SEM images of one-dimensional Sn nanowires grown on Si(100) substrate with thermal evaporation of Sn balls at 700 °C. (b) XRD pattern recorded from the Sn nanowires.

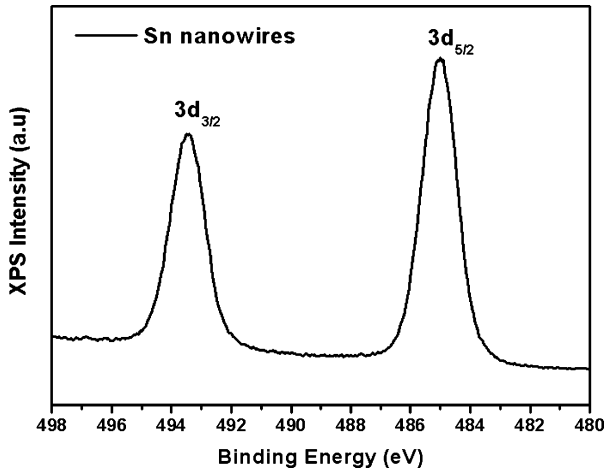

Figure 2. XPS spectrum of Sn 3d in the as-deposited Sn nanowires.

Figure 4a depicted a Sn nanowire with a winding amorphous tip, which might be attributed to the sudden termination of feeding vapor as the evaporation was ceased. The corresponding SAED pattern recorded perpendicular to the nanowire axis may be indexed to the [010] zone axis of the single-crystalline β-Sn. The high-resolution TEM image of the marked region in Figure 4a was shown in Figure 4c. The clear lattice fringes in the HRTEM image confirmed the high crystallinity of the Sn nanowire. This lattice image clearly revealed the (101) and (200) lattice planes of β-Sn with d spacings of 0.27 and 0.29 nm, respectively. The axis of the nanowire was found to be parallel to the [200] direction, indicating that the Sn nanowire was grown along the [200] direction, which is consistent with the result

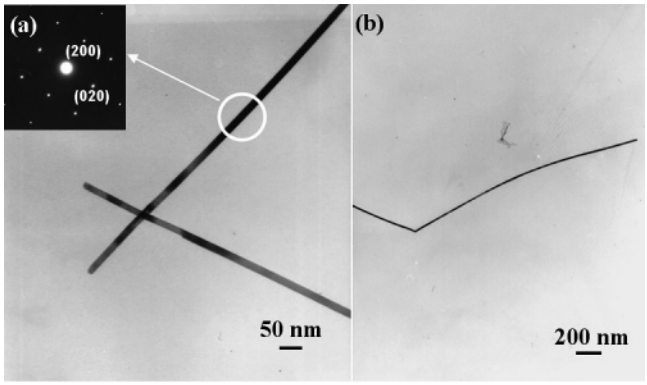

Figure 3. (a) TEM image and the inserted corresponding SAED pattern of the single-crystalline Sn nanowires. (b) Low-magnification TEM image of a single Sn nanowire revealing the uniformity of nanowire diameter along the nanowire length.

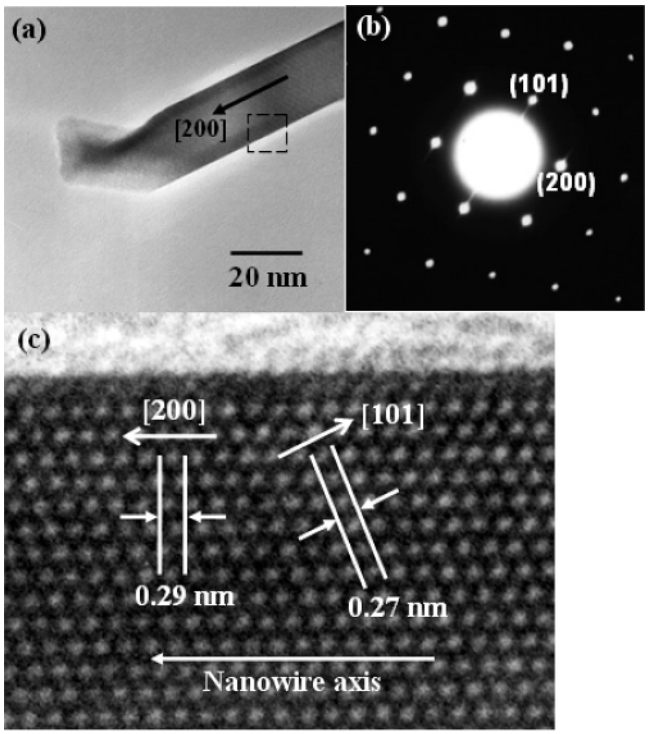

Figure 4. (a) Low-magnification TEM image of the Sn nanowire grown with the thermal evaporation of Sn balls at 700 °C. (b) and (c) corresponding SAED pattern and HRTEM images of the marked region in (a).

obtained by Tian et al.,[20] who grew tin nanowires electrochemically in polycarbonate templates.

For the as-deposited Sn nanowries, most of them possessed the perfect single crystallinity, without any commonly encountered defects such as stacking faults and dislocations, along the growth direction and terminated with the well-defined crystalline tips, as shown in Figure 5a. The lattice-resolved image of the tip region marked in Figure 5a was shown in Figure 5b. Lattice fringes corresponding to the {200} planes of β-Sn with d spacings of 0.29 nm were observed. The exposed facet of the terminated tip of the Sn nanowire, perpendicular to the nanowire axis, can be indexed as the {200} plane. We proposed that this exposing {200} plane is more unstable than any other planes and is more likely to accommodate feeding Sn vapors. The HRTEM image of the marked stem region of Figure 5a was shown in Figure 5c. An identical arrangement of lattice fringes to that at the tip region with the growing direction of [200]

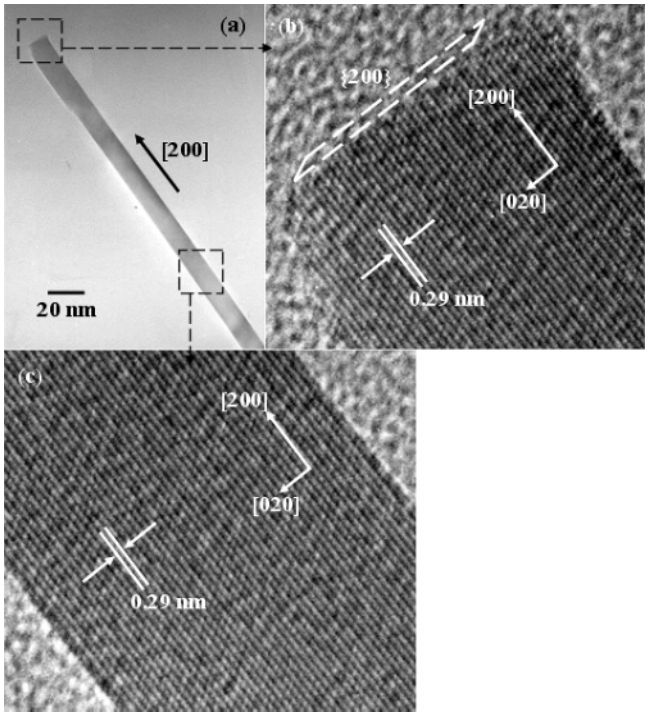

Figure 5. (a) TEM image of a single Sn nanowire with the well-defined crystalline tip. (b) and (c) HRTEM images of the tip and stem regions marked in (a), respectively.

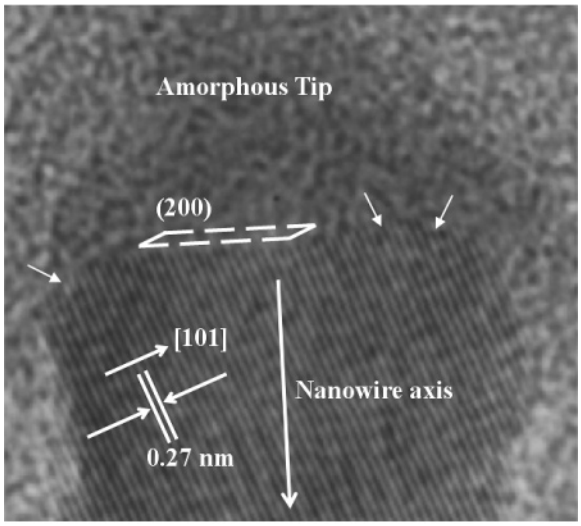

Figure 6. HRTEM image of a single Sn nanowire with an amorphous tip. Lattice fringes revealed the (101) lattice plane with d spacing of 0.27 nm.

was found. One expects atoms of the feeding vapor to strike the nanowire near the plane of least thermodynamic stability, leading to the growth of the nanowire in a preferred direction perpendicular to that specific plane. The exposing {200} plane at the tip of the Sn nanowire and the [200] direction along the nanowire axis were consistent with the above logics.

Some of the Sn nanowires were terminated with amorphous tips, resulting from the sudden cease of feeding Sn vapors. Figure 6 showed the HRTEM image of a single Sn nanowire with an amorphous tip. The interface between the amorphous and crystalline domains exhibited mostly the (200) crystallographic plane, and some microtwins attributable to the sudden end of feeding vapors existed (indicated by the inserted arrows). It may be argued that the as-prepared Sn nanowires suffered from the oxygen attack in ambient air under room temperature.

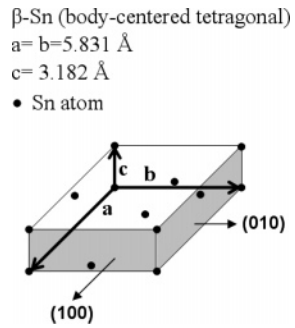

Figure 7. Crystallographic structure of body-centered tetragonal β-Sn.

TEM-EDS analysis showed that the amorphous tip of the nanowires was composed of Sn and an insignificant amount of oxygen, which probably came from the oxygen contained in the background carbon film of copper grids. Besides, at the stem regions of the nanowires the lattice-resolved image shown in Figure 4c, 5, and 6 revealed the well-defined atomic arrangement and uniform interlayer spacings corresponding to those of metallic Sn, instead of SnO or SnO_2. It was thus believed that the as-prepared nanowires were not oxidized in ambient air under room temperature. Moreover, a single set of electron diffraction pattern, which can be indexed to single-crystalline β-Sn, observed in our samples also confirmed the nanowire composition of metallic Sn and the absence of its oxides.

There have been several proposed mechanisms for the growth of nanowires, including vapor−liquid−solid (VLS),[21] solution−liquid−solid (SLS),[22] oxide-assisted growth (OAG),[23] and screw dislocation[24] mechanisms. However, none of the above mechanisms seemed suitable to explain the growth of Sn nanowires produced in the present work. First, no additional metals were employed as the catalyst in our PVD process, and both SEM and TEM images showed that no catalyst heads were found at the tips of the nanowires. As a result, the catalyst-induced VLS and SLS mechanism may be ruled out. Second, the evaporation process was carried out in the atmosphere of high-purity nitrogen, the absence of oxygen then excluded the possibility of OAG mechanism. Also, because no apparent built-in screw dislocations[15,24b] were observed in the as-deposited Sn nanowires or on the Si (100) substrate surface, the formation of Sn nanowires was not likely due to the dislocation effect. It is likely that the growth of Sn nanowires follows the mechanism similar to the vapor−solid (V−S) mechanism.[14,25−27] At the beginning, the Sn vapors were generated from the thermal evaporation of Sn balls at 700 °C. As carried by the inert nitrogen gas to the downstream regions of lower temperatures (about 210 °C), the Sn vapors started to condense on the substrate surface and crystallize. A competition in growth rate among different crystallographic planes started at the initial stage of crystallization, and once the condition at which the anisotropic one-dimensional growth was favored occurred, the feed Sn atoms started to strike on a specific favorable advancing plane to invoke and continue the one-dimensional growth, leading to formation of nanowires. Crystallographic planes possessing relatively higher surface free energies are thermodynamically more unstable, and vulnerable to attack of external atoms. The surface free energy of a specific crystallographic plane (G_{hkl}) may be expressed as $G_{hkl} = \mu_i \times n_{hkl}$, where μ_i is the chemical potential of the species and n_{hkl} is the atom number located on the (hkl) plane.[28] For the crystallographic structure of tetragonal β-Sn (as shown in Figure 7), the {100} planes (including both (100) and (010) planes) possess the highest atom numbers per unit area (0.2695 atoms/Å^2), and thus the highest surface free energy per unit area. In other words, the {100} planes of tetragonal β-Sn are thermodynamically most unstable and thus one expects the fastest growth rate along the {100} planes, leading to the preferential growth habit along the [100] direction once the anisotropic growth condition is met. The most intensive diffraction signal of the (200) plane and the growth direction of [200] along the axis of Sn nanowires observed in the XRD and HRTEM analyses, respectively, were consistent with the above argument.

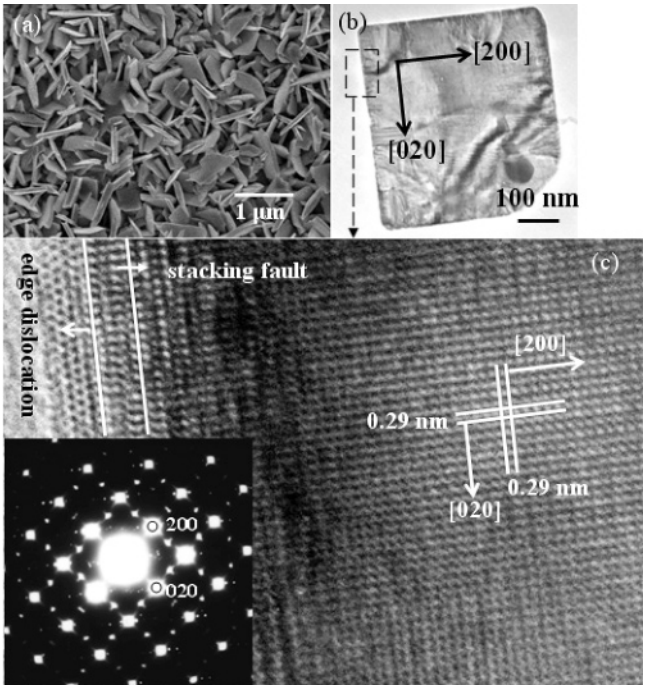

Figure 8. (a) and (b) SEM and TEM images, respectively of the as-deposited square-shaped Sn nanostructure collected in the region of a lower temperature of 180 °C. (c) HRTEM image in the edge region as marked in (b). The inserted SAED pattern was recorded along the [001] zone axis.

For the vapor−solid (V−S) mechanism that leads to the formation of one-dimensional nanostructures, the supersaturation ratio of the condensing species in the gas plays a key role.[1,15,24b] To enable anisotropic growth to form whiskers or nanowires, the supersaturation ratio of the condensing species must be maintained below some critical value, above which two-dimensional or even isotropic growth occurs. That is, a low supersaturation ratio is required for anisotropic growth, whereas a medium supersaturation ratio leads to growth of bulk crystals. At high supersaturation ratios, homogeneous nucleation in the vapor phase results in powder formation.

To further investigate the effect of supersaturation ratio on the resulting morphology, we collected deposits formed in the regions of lower temperatures (180 °C) to compare to the Sn nanowires collected in the regions of relatively higher temperatures (210 °C). Square-shaped Sn crystals were found in the lower temperature region, as shown in Figure 8a. The TEM image shown in Figure 8b revealed that the geometrical shape of the Sn nanostructures was square with a typical width of about 450 nm. The lattice-resolved image and the corresponding SAED pattern in the edge region as marked in Figure 8b were shown in Figure 8c. The growth directions of the nanosquares can be indexed along the two square edges to be the two equivalent [200] and [020], according to the lattice fringes of the {200} planes. The d spacings in both growth planes were identical with a value of 0.29 nm. The competition in growth rate between the (200) and (020) planes accounted for the formation of the two-dimensional square-shaped Sn nanostruc-

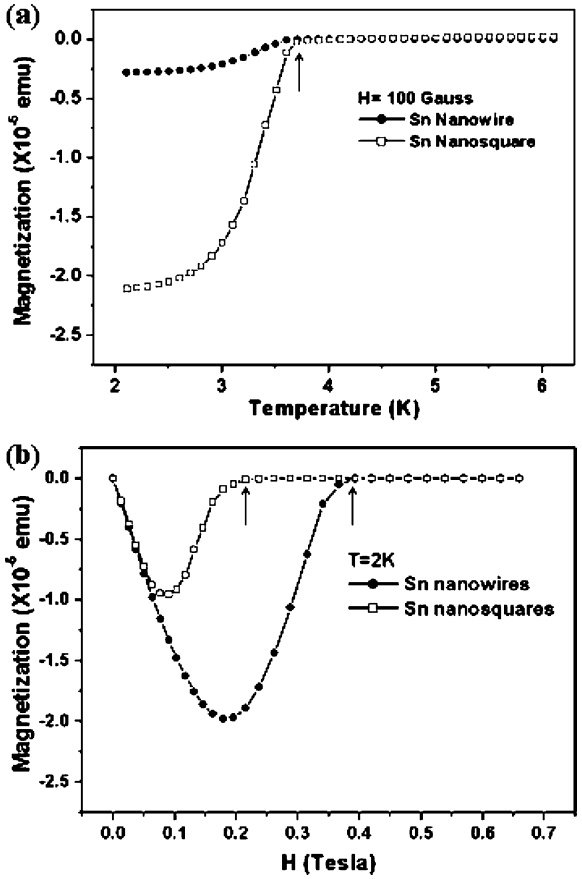

Figure 9. (a) Magnetization versus temperature curve conducted at a magnetic field of 100 G, and (b) magnetization versus magnetic field curve conducted at 2 K for both Sn nanowires and Sn nanosquares.

tures. It was believed that the critical supersaturation ratio varies as the growth conditions (such as the growth temperature and pressure) change, and its value increases rapidly with decreasing growth temperature.[15] The low-temperature region of 180 °C possessed higher supersaturation ratio, as compared to that of the relatively higher temperature region of 210 °C. And this relatively higher supersaturation ratio enabled crystal growth in two preferred directions, instead of one, resulting in formation of square-shaped Sn nanostructures.

The magnetization measurement of the deposits was also conducted to investigate the superconductivity properties of the Sn nanostructures. Figure 9a depicted the temperature-dependent magnetization data for Sn nanowires and Sn nanosquares measured with an applied magnetic field of 100 G. The data showed the typical diamagnetic behavior, an indication of superconductivity, at temperatures below the transition temperature of 3.7 K (as indicated by the inserted arrow). This transition temperature of 3.7 K was very close to that of bulk β-Sn (3.73 K).[20,29] It has been demonstrated that single-crystalline superconductors, with structural characteristic length smaller than the corresponding temperature-dependent coherence length, do not experience the significant suppression in superconducting transition temperature commonly observed for polycrystalline or amorphous superconductors.[20] The structural characteristic lengths of both Sn nanowires (10−20 nm in diameter) and Sn nanosquares (50−100 nm in thickness as determined from close-up SEM images) produced in the present work are smaller than the coherence length of bulk Sn at 0K (∼200 nm), but the suppression in superconducting transition temperature appeared to be negligible because of the single crystallinity of both nanoswires and nanosquares.

The magnetization data of the deposits as a function of the applied magnetic field at 2 K were shown in Figure 9b. The working magnetic field ranges for superconductivity of Sn nanowires and Sn nanosquares were quite broad. The onset critical magnetic fields, as indicated by the inserted arrows, were found to be around 0.39 and 0.21 T for Sn nanowires and Sn nanosquares, respectively, an order of magnitude higher than that of bulk β-Sn.[29] Note that, because the mass of the nanowires and nanosquares were hard to be determined precisely, the magnetization data were not normalized with the mass of the samples.

Conclusions

In conclusion, a noncatalytic and template-free vapor transport process has been employed to prepare single-crystalline Sn nanowires. The Sn nanowires were with a diameter of 10−20 nm and grew to several micrometers in length. Two-dimensional square-shaped nanostructures were found to form in the region of lower deposition temperatures. The rich morphology may be attributed to the competition in growth rate among different crystallographic planes. Magnetization measurements showed that the critical magnetic fields for both Sn nanowires and Sn nanosquares increased significantly as compared to that of bulk Sn. The synthesis of the single-crystalline 1-D metal nanowires and 2-D metal nanosquares may provide new possibilities for the systematic understanding of fundamental phenomena arising from this particular dimensionality, especially for metallic materials.

Acknowledgment. We gratefully acknowledge the support of the National Science Council of the Republic of China under grant NSC 92-2214-E-007-017.

References and Notes

(1) Xia, Y.; Yang, P.; Sun, Y.; Wu, Y.; Mayers, B.; Gates, B.; Yin, Y.; Kim, F.; Yan, H. *Adv. Mater.* **2003**, *15*, 353.
(2) Hu, J.; Odom, T. W.; Lieber, C. M. *Acc. Chem. Res.* **1999**, *32*, 435.
(3) Kovtyukhova, N. I.; Martin, B. R.; Mbindyo, J. K. N.; Smith, P. A.; Razavi, B.; Mayer, T. S.; Mallouk, T. E. *J. Phys. Chem. B* **2001**, *105*, 8762.
(4) Lin, Y.-M.; Cronin, S. B.; Ying, J. Y.; Dresselhaus, M. S. *Appl. Phys. Lett.* **2000**, *76*, 3944.
(5) Chou, S. Y.; Wei, M. S.; Krauss, P. R.; Fischer, P. B. *J. Appl. Phys.* **1994**, *76*, 6673.
(6) Walter, E. C.; Ng, K.; Zach, M. P.; Penner, R. M.; Favier, F. *Microelectron. Eng.* **2002**, *61*−*62*, 555.
(7) Keating, C. D.; Natan, M. J. *Adv. Mater.* **2003**, *15*, 451.
(8) Tian, M.; Wang, J.; Kurtz, J.; Mallouk, T. E.; Chan, M. H. W. *Nano Lett.* **2003**, *3*, 919.
(9) Wang, J.; Tian, M.; Mallouk, T. E.; Chan, M. H. W. *J. Phys. Chem. B* **2004**, *108*, 841.
(10) Sauer, G.; Brehm, G.; Schneider, S.; Nielsch, K.; Wehrspohn, R. B.; Choi, J.; Hofmeister, H.; Gosele, U. *J. Appl. Phys.* **2002**, *91*, 3243.
(11) Zhang, Q.; Li, Y.; Xu, D.; Gu, Z. *J. Mater. Sci. Lett.* **2001**, *20*, 925.
(12) Han, Y.-J.; Kim, J. M.; Stucky, G. D. *Chem. Mater.* **2000**, *12*, 2068.
(13) Vaddiraju, S.; Chandrasekaran, H.; Sunkara, M. K. *J. Am. Chem. Soc.* **2003**, *125*, 10792.
(14) Wang, Y.; Zhang, L.; Meng, G.; Liang, C.; Wang, G.; Sun, S. *Chem. Commun.* **2001**, 2632.
(15) (a) Sears, G. W. *Acta Metall.* **1955**, *3*, 361. (b) Sears, G. W. *Acta Metall.* **1955**, *3*, 367.
(16) Kolmakov, A.; Zhang, Y.; Moskovits, M. *Nano Lett.* **2003**, *3*, 1125.
(17) Hellmich, W.; Braunmühl, C. B.; Müller, G.; Sberveglieri, G.; Berti, M.; Perego, C. *Thin Solid Films* **1995**, *263*, 231.
(18) Huh, M.-Y.; Kim, S.-H.; Ahn, J.-P.; Park, J.-K.; Kim, B.-K. *Nanostruct. Mater.* **1999**, *11*, 211.
(19) Casella, M.; Siri, G. J.; Santori, G. F.; Ferretti, O. A. *Langmuir* **2000**, *16*, 5639.
(20) Tian, M.; Wang, J.; Snyder, J.; Kurtz, J.; Liu, Y. *Appl. Phys. Lett.* **2003**, *83*, 1620.

(21) (a) Morales, M.; Lieber, C. M. *Science* **1998**, *279*, 208. (b) Wu, Y.; Yang, P. *J. Am. Chem. Soc.* **2001**, *123*, 3165.
(22) (a) Davidson, F. M.; Schricker, A. D.; Wiacek, R. J.; Koegel, B. A. *Adv. Mater.* **2004**, *16*, 646. (b) Yu, H.; Buhro, W. E. *Adv. Mater.* **2003**, *15*, 416.
(23) Zhang, R.-Q.; Lifshitz, Y.; Lee, S.-T. *Adv. Mater.* **2003**, *15*, 635.
(24) (a) Dong, L.; Gushtyuk, T.; Jiao, J. *J. Phys. Chem. B* **2004**, *108*, 1617. (b) Wolfe, E. G.; Coskren, T. D. *J. Am. Ceram. Soc.* **1965**, *21*, 279.
(25) Pan, Z. W.; Dai, Z. R.; Wang, Z. L. *Science* **2001**, *291*, 1947.
(26) Jiang, Y.; Meng, X.-M.; Yiu, W.-C.; Liu, J.; Ding, J.-X.; Lee, C.-S.; Lee, S.-T. *J. Phys. Chem. B* **2004**, *108*, 2784.
(27) Zhang, J.; Jiang, F.; Zhang, L. *J. Phys. Chem. B* **2004**, *108*, 7002.
(28) Tiller, W. A. *The Science of Crystallization: Microscopic Interfacial Phenomena*; Cambridge University Press: New York, 1991.
(29) Natsik, V. D.; Soldatov, V. P.; Ivanchenko, L. G.; Kirichenko, G. I. *Low Temp. Phys.* **2004**, *30*, 253.